Depletion of PINK1 affects mitochondrial metabolism, calcium homeostasis and energy maintenance

Bavo Heeman[1,*], Chris Van den Haute[1,*], Sarah-Ann Aelvoet[1], Federica Valsecchi[2,3], Richard J. Rodenburg[3], Veerle Reumers[1], Zeger Debyser[4], Geert Callewaert[5], Werner J. H. Koopman[2], Peter H. G. M. Willems[2] and Veerle Baekelandt[1,‡]

[1]Laboratory for Neurobiology and Gene Therapy, Molecular Medicine, Katholieke Universiteit Leuven, 3000 Leuven, Flanders, Belgium
[2]Department of Biochemistry (286), Nijmegen Centre for Molecular Life Sciences, Radboud University Nijmegen Medical Centre, 6500 Nijmegen, the Netherlands
[3]Department of Pediatrics, Nijmegen Centre for Mitochondrial Disorders, Radboud University Nijmegen Medical Centre, 6500 Nijmegen, the Netherlands
[4]Laboratory for Molecular Virology and Gene Therapy, Molecular Medicine, Katholieke Universiteit Leuven and Interdisciplinary Research Centre, Katholieke Universiteit Leuven Campus Kortrijk, 8500 Kortrijk, Flanders, Belgium
[5]Research Group Neurodegeneration, Interdisciplinary Research Centre, Katholieke Universiteit Leuven Campus Kortrijk, 8500 Kortrijk, Flanders, Belgium

*These authors contributed equally to this work
‡Author for correspondence (Veerle.Baekelandt@med.kuleuven.be)

Accepted 2 December 2010
Journal of Cell Science 124, 1115-1125

doi:10.1242/jcs.078303

Summary

Loss-of-function mutations in the gene encoding the mitochondrial PTEN-induced putative kinase 1 (PINK1) are a major cause of early-onset familial Parkinson's disease (PD). Recent studies have highlighted an important function for PINK1 in clearing depolarized mitochondria by mitophagy. However, the role of PINK1 in mitochondrial and cellular functioning in physiological conditions is still incompletely understood. Here, we investigate mitochondrial and cellular calcium (Ca^{2+}) homeostasis in PINK1-knockdown and PINK1-knockout mouse cells, both in basal metabolic conditions and after physiological stimulation, using unbiased automated live single-cell imaging in combination with organelle-specific fluorescent probes. Our data reveal that depletion of PINK1 induces moderate fragmentation of the mitochondrial network, mitochondrial membrane depolarization and increased production of reactive oxygen species. This results in reduced uptake of Ca^{2+} by mitochondria after physiological stimulation. As a consequence, cells with knockdown or knockout of PINK1 display impaired mitochondrial ATP synthesis, which is exacerbated under conditions of increased ATP demand, thereby affecting cytosolic Ca^{2+} extrusion. The impairment in energy maintenance was confirmed in the brain of PINK1-knockout mice by in vivo bioluminescence imaging. Our findings demonstrate a key role for PINK1 in the regulation of mitochondrial homeostasis and energy metabolism under physiological conditions.

Key words: Mitochondria, Live cell imaging, Parkinson's disease, Lentiviral vector

Introduction

Parkinson's disease (PD) results from a progressive loss of dopaminergic neurons in the substantia nigra and is the most common age-related neurodegenerative movement disorder. The molecular mechanisms underlying the neuronal degeneration remain poorly understood, although a growing body of evidence implicates mitochondrial dysfunction in PD pathogenesis (Abou-Sleiman et al., 2006). Exposure to mitochondrial toxins, such as 1-methyl-4-phenyl-1,2,3,6-tetrahydropyridine (MPTP), resulted in PD-like symptoms in rodents and humans (Langston et al., 1983). Then, post-mortem studies reported deficiency of mitochondrial complex I in some sporadic PD patients (Schapira et al., 1989) and an increased number of somatic mitochondrial DNA mutations in nigral neurons (Bender et al., 2006). The strongest evidence, however, came from the discovery of gene mutations in mitochondrial proteins leading to inherited forms of PD (Gasser, 2009). Mutations in *PINK1* were initially identified in three families with autosomal-recessive PD (Valente et al., 2004). Since then, many mutations have been found throughout *PINK1*, with the majority situated within the kinase domain. The location of these mutations and their recessive nature suggest that loss of PINK1 kinase function is responsible for disease onset (Matsuda et al., 2010).

PINK1 encodes a protein with an N-terminal mitochondrial targeting motif, a highly conserved serine-threonine kinase domain and a C-terminal autoregulatory domain. PINK1 predominantly localizes to the mitochondria (Weihofen et al., 2009; Zhou et al., 2008), suggesting a role in mitochondrial function. PINK1-deficient cells were shown to be more susceptible to apoptosis after exposure to mitochondrial toxic insults (Deng et al., 2005; Valente et al., 2004). In addition, inactivation of the *Drosophila* PINK1 ortholog induced a severe mitochondrial phenotype that consisted of mitochondrial aggregates, swollen and enlarged mitochondria and reduced ATP synthesis, both in flight muscle cells and dopaminergic neurons (Clark et al., 2006; Park et al., 2006). Furthermore, knockdown of PINK1 in mammalian cells, as well as PINK1 mutations in fibroblasts from patients with PD, have been associated with (sometimes contradictory) changes in mitochondrial morphology and mitochondrial membrane potential (Exner et al., 2007; Lutz et al., 2009; Sandebring et al., 2009; Weihofen et al., 2009; Wood-Kaczmar et al., 2008).

Journal of Cell Science

In the present study, we investigated mitochondrial metabolism and cellular Ca^{2+} homeostasis using unbiased automated live single-cell imaging. We studied dynamic processes such as mitochondrial Ca^{2+} uptake, ATP synthesis and cytosolic Ca^{2+} metabolism in resting and stimulated conditions. We demonstrate that silencing of *Pink1* induces moderate mitochondrial fragmentation and depolarization of the mitochondrial membrane potential, which results in impaired mitochondrial Ca^{2+} influx. As a consequence, energy maintenance becomes problematic, especially under conditions of increased energy demand. These findings suggest a physiological role for PINK1 in mitochondrial homeostasis.

Results

Depletion of PINK1 by RNAi-mediated knockdown in mouse cells and by the generation of PINK1-knockout mice

We investigated the function of PINK1 by mimicking the loss of function that results from the clinical *PINK1* mutations using two complementary strategies. First, we induced stable knockdown (KD) of PINK1 in mouse neuroblastoma (N2a) cells and in primary mouse embryonic fibroblasts (MEFs) using two lentiviral vectors (LVs) expressing a miRNA30-based short-hairpin sequence (sh1PINK1 or sh2PINK1) against mouse *Pink1*. LV-sh1PINK1 and LV-sh2PINK1 decreased levels of *Pink1* mRNA in selected cells by ~70% and ~85%, respectively (supplementary material Fig. S1A,B).

Second, we generated PINK1-knockout (KO) mice by targeted deletion of exon 1 (supplementary material Fig. S1C,D). Loss of *Pink1* mRNA expression in brain and primary MEFs was confirmed by quantitative RT-PCR (supplementary material Fig. S1E). Cell growth was not detectably altered in PINK1-KO MEFs (supplementary material Fig. S1F), confirming that any phenotypical differences observed are not due to differences in growth rate. Also, there was no evidence of apoptosis upon exposure to the different fluorescent probes and substrates used in further experiments (data not shown).

Loss of PINK1 induces moderate mitochondrial fragmentation in mammalian cells

Silencing of the *Drosophila* PINK1 ortholog is associated with mitochondrial enlargement and disintegration (Clark et al., 2006; Park et al., 2006). However, in PINK1-depleted mammalian cells, mitochondrial morphology changes are either absent or relatively small, and point to fission rather than fusion (Dagda et al., 2009; Exner et al., 2007; Morais et al., 2009; Sandebring et al., 2009). To assess the effect of silencing of *Pink1* on mitochondrial morphology in an unambiguous way, we used live imaging of cells loaded with the mitochondrial fluorescent dye TMRM (Fig. 1A). Unbiased quantification in a large population of cells revealed a 25% decrease in mitochondrial form factor (F), a combined measure of mitochondrial length and degree of branching, in PINK1-KO MEFs (Fig. 1B). This effect was paralleled by a 22% decrease in mitochondrial area (A_M) and a 20% increase in the number of mitochondrial objects per cell (N_c) (Fig. 1C,D), whereas total mitochondrial mass (M_M) was identical in PINK1-KO and control MEFs (Fig. 1E). Similar results were obtained after RNAi-based silencing of *Pink1* in undifferentiated N2a cells and in primary MEFs (Fig. 1B–E). However, because TMRM uptake by the mitochondria is dependent on the membrane potential ($\Delta\psi$), we also determined the mitochondrial mass in a $\Delta\psi$-independent manner by high-content quantification of total TOM-20 immunofluorescence per cell. This analysis showed an 11% increase in mitochondrial mass in PINK1-KO cells (Fig. 1F). Taken together, these data indicate that depletion of PINK1 causes moderate fragmentation of functional mitochondria in mammalian cells, and a slight accumulation of depolarized mitochondria.

PINK1-deficient cells display increased levels of reactive oxygen species

Mitochondria are an important source of reactive oxygen species (ROS) and altered levels of ROS indicate changes in mitochondrial physiology (Forkink et al., 2010). To assess ROS levels, we used live cell imaging of MEFs pre-incubated with hydroethidine (HEt) (Koopman et al., 2005). Intracellularly, HEt reacts with ROS to form fluorescent, positively charged 2-hydroxyethidium and ethidium products. Subcellular quantification of these HEt oxidation products in mitochondria-rich regions revealed an increase of about 15% in both PINK1-KD and PINK-KO MEFs (Fig. 1G). Replacing glucose by galactose in the culture medium to stimulate mitochondrial energy metabolism, further increased HEt oxidation in PINK1-KD and PINK1-KO MEFs.

Silencing of PINK1 affects the mitochondrial membrane potential

Maintenance of a sufficiently large, inside-negative $\Delta\psi$ across the mitochondrial inner membrane is crucial for mitochondrial function and integrity. To assess $\Delta\psi$, we quantified the average mitochondrial fluorescence intensity of the cationic TMRM (Koopman et al., 2008; Nicholls and Ward, 2000). When mitochondrial accumulation of TMRM exceeds a certain concentration, autoquenching is induced, resulting in a transient increase in TMRM signal (due to dequenching) upon $\Delta\psi$ depolarization. Control experiments revealed that addition of the mitochondrial uncoupler carbonylcyanide-p-trifluoromethoxyphenylhydrazone (FCCP) induced an immediate decrease without a transient increase in TMRM fluorescence (supplementary material Fig. S2). Therefore, TMRM fluorescence is not autoquenched in our experiments. Subsequent single-cell measurements revealed a significant reduction in mitochondrial TMRM pixel intensity in PINK1-KD and PINK1-KO MEFs (Fig. 1A and Fig. 2A), supporting the conclusion that mitochondria in PINK1-deficient cells have a depolarized $\Delta\psi$.

PINK1-deficient cells have normal respiratory complexes

The mitochondrial membrane potential is maintained by complex I to complex IV of the oxidative phosphorylation (OXPHOS) system. These complexes use the energy obtained from the oxidation of NADH and $FADH_2$ to extrude protons from the matrix into the intermembrane space. The electrochemical proton gradient generated this way drives the ATP production at complex V. To determine whether $\Delta\psi$ depolarization in PINK1-deficient cells was related to malfunctioning of the OXPHOS system, we determined the maximal activity of individual OXPHOS complexes in mitochondria-enriched fractions. Additionally, we analyzed the activity of citrate synthase (CS), a key enzyme of the tricarboxylic acid (TCA) cycle. All enzymes displayed normal activity in PINK1-KD and PINK1-KO MEFs (Fig. 2B). Similar results were obtained with PINK1-deficient N2a cells (supplementary material Fig. S3A). The absence of large changes in CS activity is compatible with our finding that PINK1 deficiency only slightly affects mitochondrial mass. Native gel electrophoresis of mitochondrial fractions followed by either western blotting or IGA measurement again revealed

similar amounts and activities of complex I in PINK1-KD, PINK1-KO and control MEFs (Fig. 2C). Western blot analysis further showed that the other OXPHOS complexes were also normally expressed in PINK1-KD and PINK1-KO MEFs (supplementary material Fig. S3B). In addition, we quantified NAD(P)H autofluorescence in mitochondria-enriched regions of individual MEFs as a functional readout for cellular metabolic activity. Similar levels of NAD(P)H autofluorescence were observed in PINK1-KD and PINK1-KO MEFs as in control cells (Fig. 2D). Acute treatment with the specific complex I inhibitor rotenone increased the autofluorescence signal in PINK1-deficient MEFs to the same level as in controls. Together, these data indicate that PINK1 deficiency does not alter OXPHOS expression and/or activity.

Depletion of PINK1 results in impairment of stimulated mitochondrial Ca^{2+} uptake

Many extracellular stimuli exert their effect through an increase in cytosolic calcium ($[Ca^{2+}]_C$) mediated by the stimulated influx of extracellular Ca^{2+} and/or the stimulated release of Ca^{2+} from intracellular stores, predominantly the endoplasmic reticulum (ER). Depending on their membrane potential and energization state, mitochondria take up a greater or lesser part of the Ca^{2+} that enters the cytosol.

To measure mitochondrial calcium ($[Ca^{2+}]_M$), cells were stably transduced with a LV encoding mitochondrial aequorin (mtAEQ) which emits visible light in a Ca^{2+}-concentration-dependent manner (Rizzuto et al., 1992). Stimulation of N2a cells and primary MEFs caused a rapid increase in $[Ca^{2+}]_M$ as a result of Ca^{2+} influx via the electrogenic Ca^{2+} uniporter. The peak value was significantly decreased by about 20% in PINK1-KD N2a cells compared with different control cell lines (from 91.35±2.74 µM in non-transduced cells, 86.95±3.08 µM in LV-blasti cells and 86.91±1.54 µM in sh1PINK1MM cells to 70.28±1.19 µM and 65.8±2.49 µM in sh1PINK1 and sh2PINK1 cells, respectively) (Fig. 3A,B). A similar reduction in peak $[Ca^{2+}]_M$ increase was observed in PINK1-KD primary MEFs (Fig. 3C,D). Complete absence of PINK1 did not

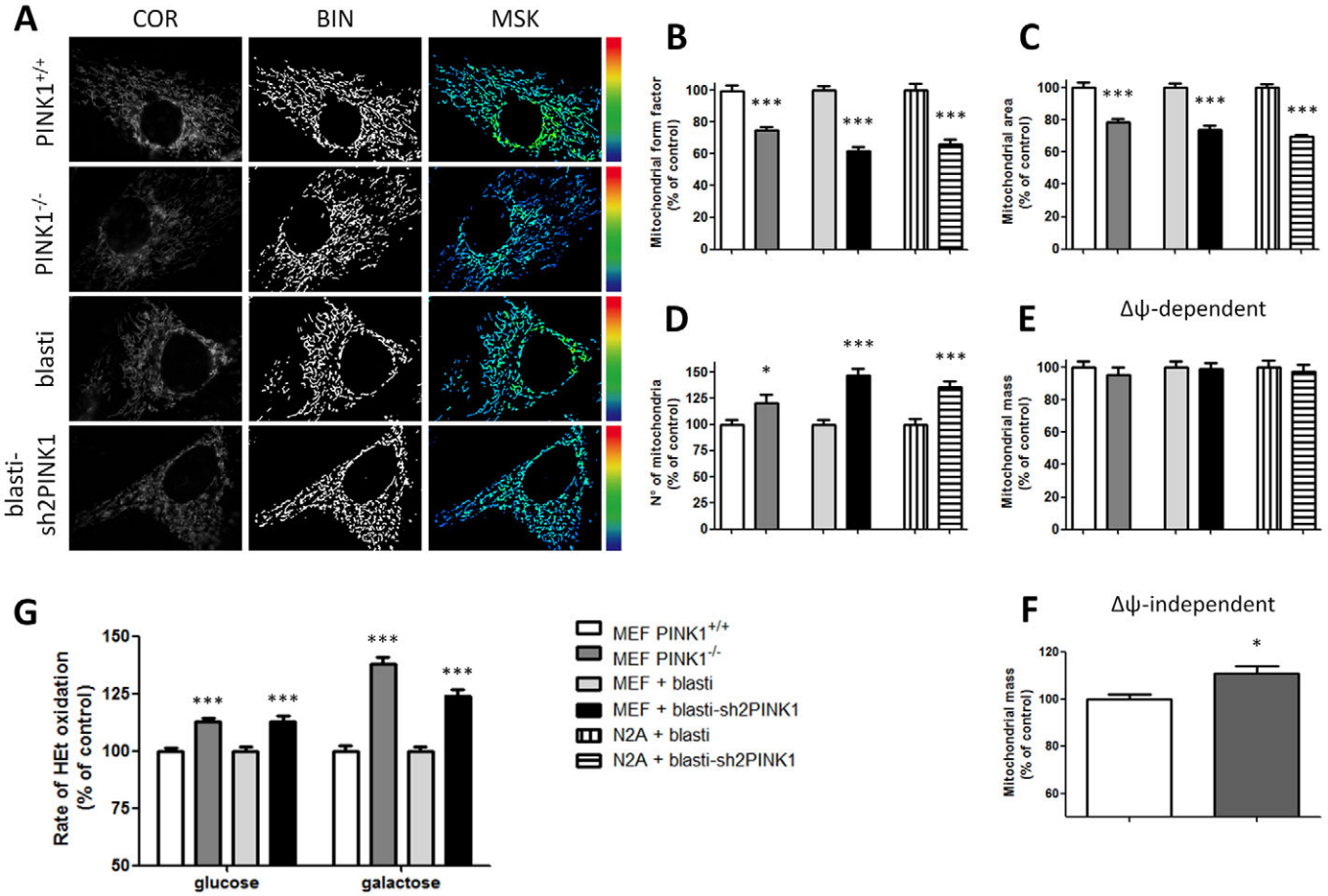

Fig. 1. Mitochondrial morphology and ROS production in PINK1-depleted cells. (**A**) Typical images of mitochondria from primary MEFs loaded with TMRM. Background-corrected raw microscopy images (COR) were converted in binary images (BIN) using an automated sequential image processing algorithm. Masking of the COR image with the BIN image resulted in an intensity-coded image of the mitochondrial objects (MSK). The latter was used for automated quantification of mitochondrial morphology and TMRM pixel intensity. Color-coded scale bar indicates the intensity of TMRM fluorescence from blue (low intensity) to red (high intensity). (**B**–**E**) Quantitative analysis of mitochondrial parameters in PINK1-depleted MEFs and N2A cells vs control cells: mitochondrial form factor (B), mitochondrial area (C), number of mitochondria per cell (D) and mitochondrial mass (E). Total number of objects (mitochondria) and cells analyzed: wild-type MEFs, 25,228 in 115 cells; PINK1-KO MEFs, 23,974 in 90 cells; PINK1-KD MEFs, 26,749 in 94 cells; PINK1 control MEFs, 17,314 in 88 cells; PINK1-KD N2A, 18,888 in 144 cells; control N2A, 27,590 in 129 cells. (**F**) Quantitative analysis of mitochondrial mass in fixed MEFs (n>3000 cells), using TOM-20 as a Δψ-independent mitochondrial marker. (**G**) Primary MEFs were loaded with HEt to measure mitochondrial ROS production in glucose and galactose medium in a large number of single cells (n>300 per condition); *P<0.05 vs control group, ***P<0.001 vs control group.

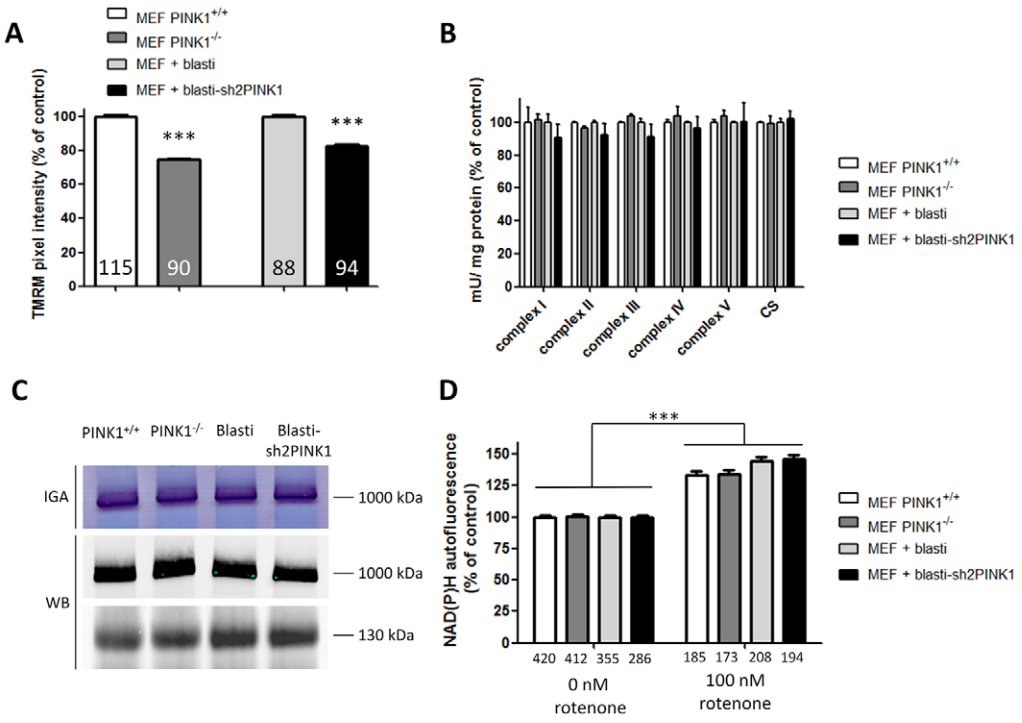

Fig. 2. Silencing of PINK1 affects mitochondrial membrane potential but not activity of the OXPHOS complex. (**A**) Primary MEFs were stained with the mitochondrial TMRM probe to determine the mitochondrial membrane potential (Fig. 1A). Quantification of the MSK image in both PINK1-KD and PINK1-KO MEFs and control cells was used to calculate average mitochondrial TMRM intensity. (**B**) Biochemical enzymatic analysis of complex I to complex V and CS in mitochondria-enriched MEF fractions. Measurements were performed in duplicate from three independent cell isolations and normalized to protein content. (**C**) Mitochondrial protein complexes of PINK1-KD, PINK1-KO and control MEFs (3×10^6 cells) were isolated, followed by gel electrophoresis. In vitro in-gel activity (IGA) was measured for complex I (upper panel) and western blotting (WB) was used to detect complex I (1000 kDa) and complex II (130 kDa) as a loading control. (**D**) Live cell imaging of NAD(P)H autofluorescence in primary MEFs. Measurements were performed in the absence and in the presence of the complex I inhibitor rotenone. Number of cells for TMRM intensity and NAD(P)H autofluorescence measurements is indicated for each column. ***P<0.001 vs corresponding control group.

further reduce the mitochondrial Ca^{2+} uptake in PINK1-KO MEFs (Fig. 3E,F). Similar values were obtained in galactose culture conditions (Fig. 3F). In all conditions tested, basal mitochondrial Ca^{2+} levels did not significantly differ between control cells and PINK1-KD or PINK1-KO cells. Pretreatment of the cells with FCCP abolished the $[Ca^{2+}]_M$ increase induced by BK or ATP (data not shown), confirming that mtAEQ localizes to the mitochondrial matrix (Visch et al., 2004).

Because the $[Ca^{2+}]_M$ data acquired involved monitoring of the luminescence in total cell populations, we next investigated the cells in more detail by means of single-cell digital microscopy. Moreover, the mtAEQ measurements described above do not allow reliable analysis of the kinetics of mitochondrial Ca^{2+} release because the decline of the mtAEQ signal might not only reflect the decrease in $[Ca^{2+}]_M$, but also the depletion of the mtAEQ – coelenterazine complex (Visch et al., 2006). Therefore, MEFs were loaded with the mitochondria-specific fluorescent Ca^{2+} indicator Rhod-2. Digital imaging microscopy of individual MEFs showed a 25% reduction of the peak increase in Rhod-2 fluorescence following ATP stimulation in PINK1-KD and PINK1-KO MEFs (Fig. 3G,H). This confirms the reduced $[Ca^{2+}]_M$ peak value observed with the mtAEQ measurements. To analyze the subsequent mitochondrial Ca^{2+} release, mono-exponential fitting of the subsequent decrease in Rhod-2 fluorescence was performed. These calculations revealed no differences between PINK1-KD or PINK1-KO MEFs and controls (blasti, $t_{1/2}$=35.13±8.14 seconds; PINK1-KD, $t_{1/2}$=34.68±4.58 seconds; PINK1 wild type, $t_{1/2}$=28.12±4.79 seconds; PINK1-KO, $t_{1/2}$=32.82±2.97 seconds), which suggests normal functioning of the mitochondrial Ca^{2+}-extrusion mechanisms in PINK1-deficient cells.

PINK1-deficient cells show decreased mitochondrial ATP synthesis

Agonist-induced increase in $[Ca^{2+}]_M$ boosts the activation of pyruvate dehydrogenase, two key regulatory dehydrogenases of the TCA cycle (2-oxoglutarate dehydrogenase and isocitrate dehydrogenase) and complex V. This in turn stimulates the OXPHOS complexes, resulting in increased mitochondrial ATP ($[ATP]_M$) synthesis (Jouaville et al., 1999; Valsecchi et al., 2009). To investigate whether the impaired mitochondrial Ca^{2+} uptake observed in the PINK1-KD and PINK1-KO cells affected $[ATP]_M$, we determined these levels in resting and stimulated cells. To measure the resting ATP levels, primary MEFs stably expressing mtLUC were perfused with D-luciferin (100 μM) and luminescence was quantified by means of photon counting. Approximately 2 minutes after the onset of D-luciferin perfusion (defined as time point t_1), comparable bioluminescence maxima were reached in PINK1-KD and control MEFs (Fig. 4A,B). However, continued monitoring of the basal $[ATP]_M$ showed a subsequent decrease to a new steady-state level (defined as time point t_2) by 22.30±2.86% in PINK1-KD MEFs and by only 3.17±0.89% in control MEFs (Fig. 4C). Comparable data were obtained in galactose medium

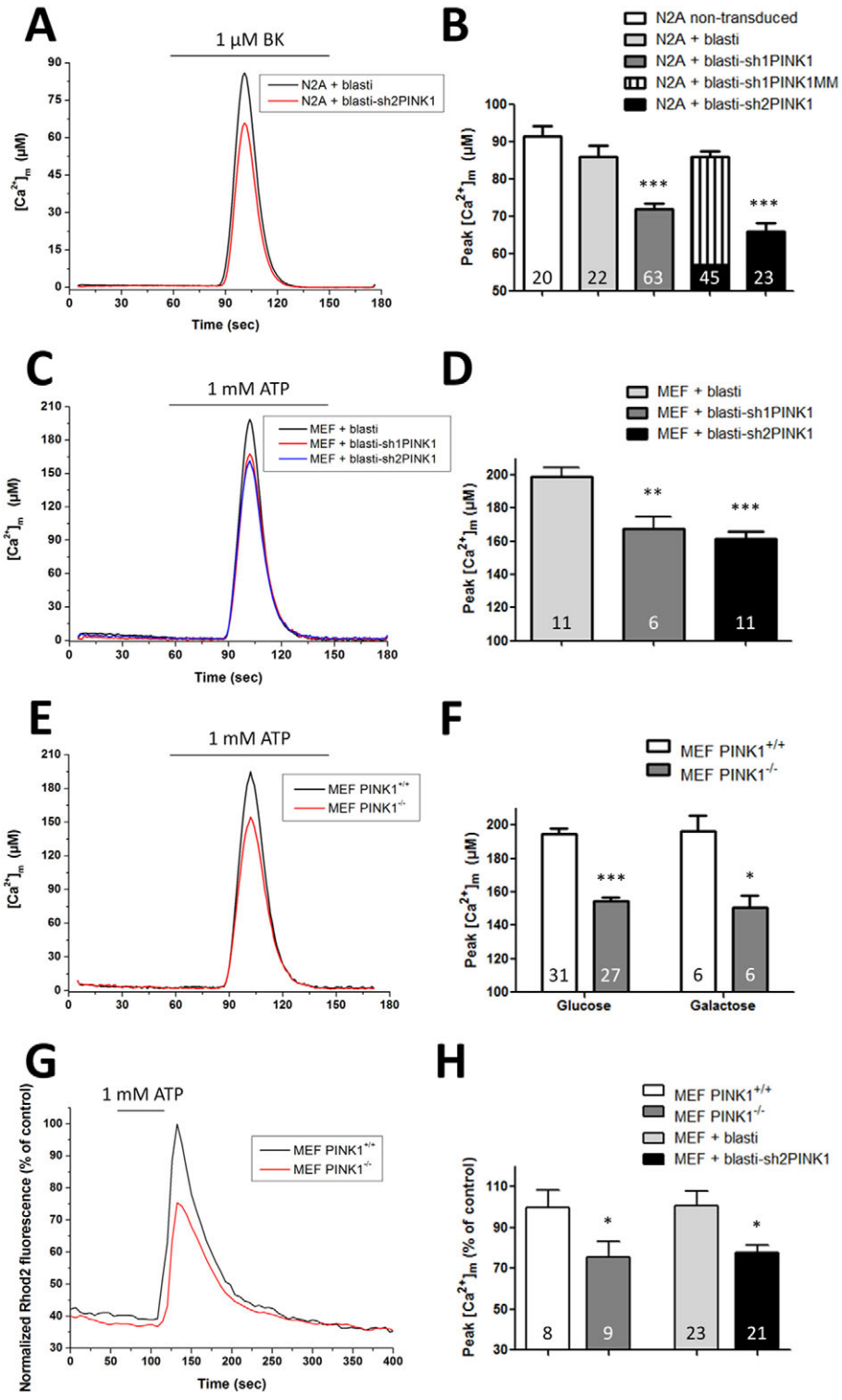

Fig. 3. Silencing of PINK1 impairs agonist-induced mitochondrial Ca^{2+} uptake in mouse N2a cells and primary MEFs. (**A**) Bradykinin-induced increase of $[Ca^{2+}]_M$ in N2a cells expressing mtAEQ. Data are shown for one control (LV-blasti) and one PINK1-KD cell line (LV-sh2PINK1). (**B**) BK-evoked $[Ca^{2+}]_M$ peak values of both N2a PINK1-KD cell lines (sh1PINK1 and sh2PINK1) compared with controls. (**C**,**D**) ATP-induced changes in $[Ca^{2+}]_M$ peak value of PINK1-KD MEFs (both sh1PINK1 and sh2PINK1) and control cells expressing mtAEQ. (**E**,**F**) Luminometric analysis of the ATP-induced peak increase of $[Ca^{2+}]_M$ in PINK1 wild-type and PINK1-KO MEFs expressing mtAEQ. Cells were cultured in medium containing glucose (25 mM) or galactose (10 mM). (**G**) Single-cell digital imaging microscopy of the ATP-induced increase of $[Ca^{2+}]_M$ in PINK1 wild-type and PINK1-KO MEFs treated with Rhod-2. (**H**) Quantification of the ATP-stimulated $[Ca^{2+}]_M$ peak increase in MEFs loaded with Rhod-2. The maximal increase obtained with untreated cells was set at 100%. Number of coverslips (A–F) or cells (G–H) is indicated for each column. **P*<0.05, ***P*<0.01 and ****P*<0.001 vs control group.

(supplementary material Fig. S4A–C). A similar decrease of 19.77±0.66% was observed in PINK1-KO MEFs, whereas control MEFs showed a decrease of only 4.40±0.37% (Fig. 4E,G). Increasing the amount of D-luciferin to 500 µM revealed differences between control MEFs (22.43±1.07%) and PINK1-KO MEFs (17.08±1.47%) at time point t_1 (Fig. 4I,J), whereas at t_2 the bioluminescence values in these cells were decreased by 11.07±0.56% and 36.89±2.16%, respectively (Fig. 4K). Together, these findings indicate that unstimulated PINK1-deficient cells are unable to maintain basal $[ATP]_M$ levels under conditions of increased ATP demand.

Next, to determine the effect of PINK1 deficiency on agonist-induced increase in mitochondrial ATP concentration, MEFs were challenged with the Ca^{2+}-mobilizing agonist ATP to induce a maximal increase in $[Ca^{2+}]_C$ and $[Ca^{2+}]_M$. Under these stimulatory conditions, PINK1-KD MEFs showed a markedly reduced $[ATP]_M$ peak (defined

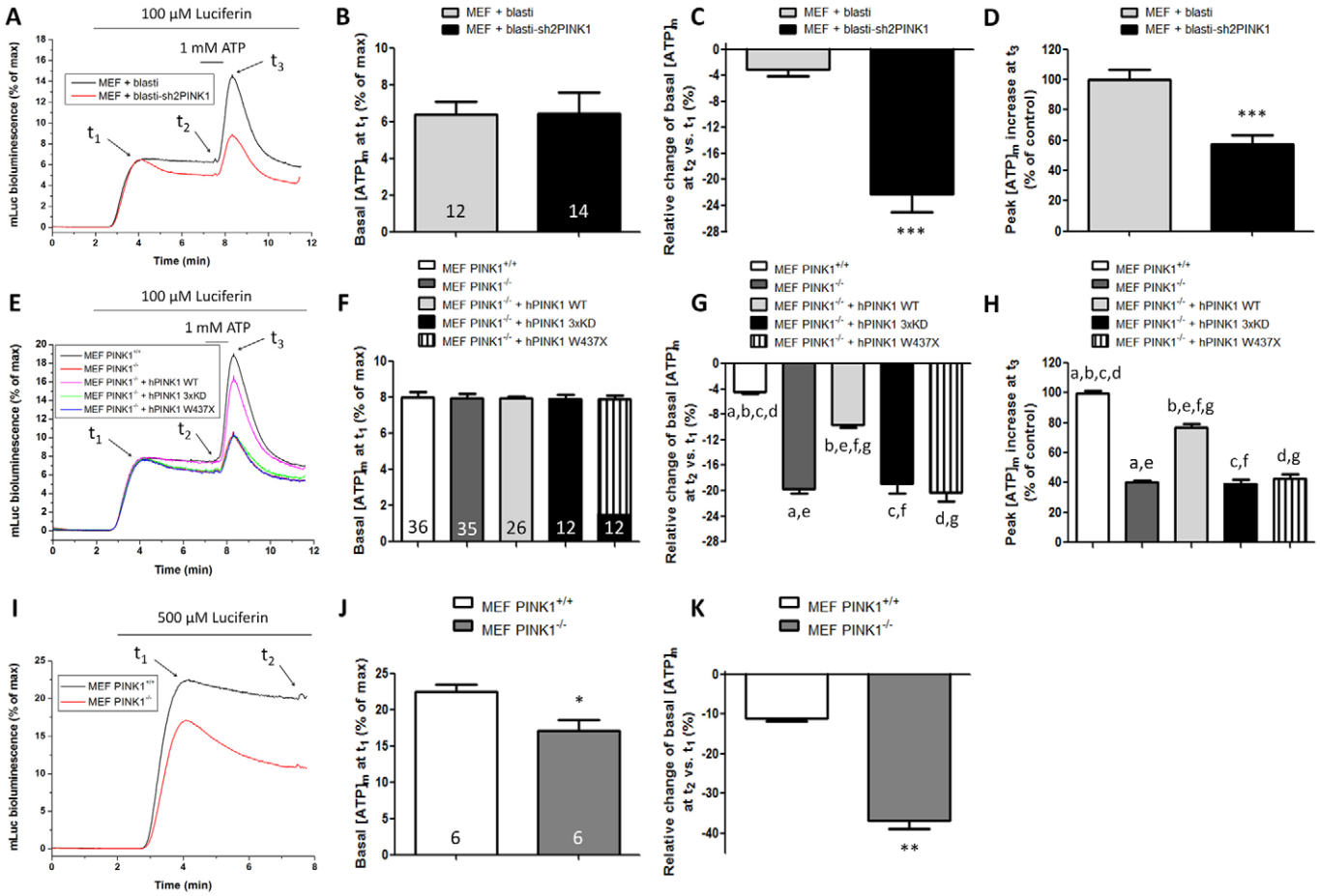

Fig. 4. Mitochondrial ATP synthesis is reduced in PINK1-deficient MEFs. Basal- and ATP-evoked increase of $[ATP]_M$ in MEFs expressing mtLUC and perfused with 100 µM or 500 µM D-luciferin. (**A**) $[ATP]_M$ measurements in control and PINK1-KD MEFs. (**B**) basal $[ATP]_M$ levels at time point t_1, (**C**) relative change of basal $[ATP]_M$ values at time point t_2, and (**D**) ATP-stimulated peak increase in $[ATP]_M$ (at time point t_3). (**E**–**H**) Luminometric analysis of $[ATP]_M$ in PINK1 wild-type and PINK1-KO MEFs, including PINK1-KO MEFs stably overexpressing human WT PINK1 or one of its mutants (3x kinase-dead and W437X). Columns labeled with the same letters show significant differences between the two conditions. (**I**) $[ATP]_M$ measurements in PINK1 wild-type and PINK1-KO MEFs perfused with 500 µM D-luciferin. Quantification of bioluminescence shows a lower basal $[ATP]_M$ level at time point t_1 (**J**) and a higher basal $[ATP]_M$ decrease at time point t_2 (**K**) in PINK1-KO MEFs compared with control cells. Number of coverslips examined is indicated on the columns. *P<0.05, **P<0.01 and ***P<0.001 vs control group.

as time point t_3) in both glucose (Fig. 4A,D) and galactose medium (supplementary material Fig. S4A,D). The agonist-induced peak increase in bioluminescence was also significantly reduced in PINK1-KO MEFs (t_3 values of 100±1.20% and 40.08±1.71% in control and PINK1-KO MEFs, respectively) (Fig. 4E,H).

To investigate the specificity of the observed mitochondrial phenotype, we determined $[ATP]_M$ following reintroduction of human WT PINK1, a PD-linked W437X PINK1 mutant or an artificial triple kinase-dead (3xKD) PINK1 mutant. Expression of human WT PINK1 and its mutants resulted in comparable PINK1 protein overexpression levels (supplementary material Fig. S5A) in nearly all cells (supplementary material Fig. S5B). Nevertheless, PINK1-KO MEFs back-complemented with human WT PINK1 showed a partial rescue of the signal at t_2 (i.e. the decrease was normalized from 19.77±0.66% to 9.58±0.45%) and at t_3 (the peak value was enhanced from 40.08±1.71% to 76.77±2.41%), whereas both PINK1 mutants completely failed to restore mitochondrial ATP synthesis (Fig. 4E–H). In control MEFs, stable overexpression of WT PINK1 or the mutants did not affect any of the parameters tested (supplementary material Fig. S4E–H).

PINK1-deficient cells display altered cytosolic Ca^{2+} metabolism under conditions of high ATP demand

Cytosolic and mitochondrial Ca^{2+} homeostasis are tightly coupled. Indeed, mitochondria control the amplitude, spatial spreading and duration of the cytosolic Ca^{2+} signal by taking up Ca^{2+} and releasing ATP to directly or indirectly fuel cytosolic Ca^{2+}-extrusion mechanisms via Ca^{2+}-ATPases of the plasma membrane (PMCA), Ca^{2+}-ATPases of the sarcoplasmic and endoplasmic reticulum (SERCA) or Na^+–Ca^{2+} exchangers of the plasma membrane. Using live cell imaging of cells loaded with the cytosolic Ca^{2+} indicator Fura-2, we next investigated whether PINK1 deficiency affected cytosolic Ca^{2+} signals.

No difference in resting $[Ca^{2+}]_C$ was observed between unstimulated PINK1-KO and control MEFs (Fig. 5A and supplementary material Table S2). Likewise, when cells were stimulated with ATP, no difference in peak $[Ca^{2+}]_C$ increase was observed. These results were reproduced in PINK1-KD MEFs (supplementary material Table S2) and N2a cells (Fig. 5B and supplementary material Table S3) and demonstrate that the observed reductions in agonist-induced mitochondrial Ca^{2+} uptake in PINK1-

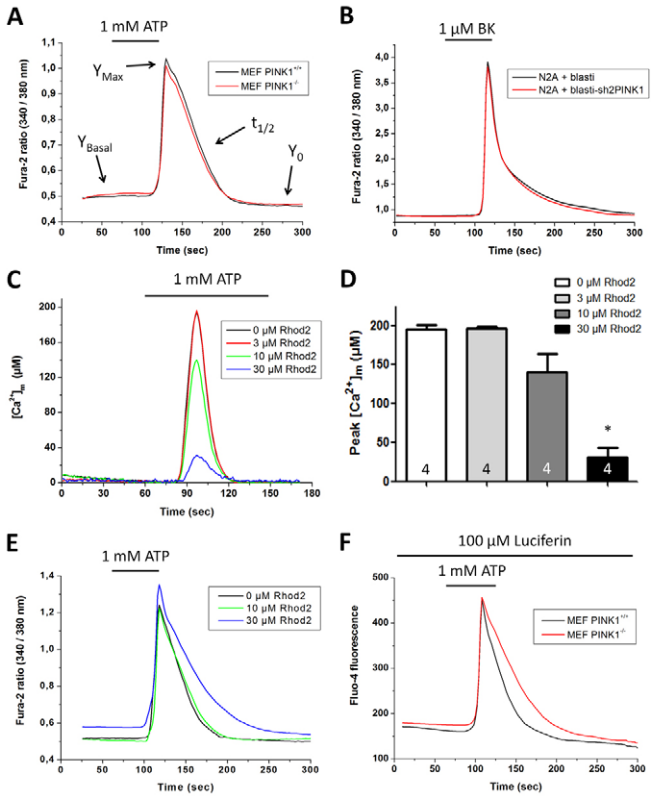

Fig. 5. Cytosolic Ca^{2+} handling is impaired in PINK1-deficient cells following increased ATP demand. (**A**,**B**) Cytosolic Ca^{2+} signaling was assessed in Fura-2-loaded primary MEFs (A) and in N2A cells (B). Four parameters were determined: basal $[Ca^{2+}]_C$ before (Y_{Basal}) and after (Y_0) agonist-induced cell stimulation, the peak $[Ca^{2+}]_C$ increase (Y_{Max}) and the kinetics ($t_{1/2}$) of cytosolic Ca^{2+} removal (see also supplementary material Tables S2 and S3). (**C**) Effect of increasing concentrations Rhod-2 (0, 3, 10 and 30 µM) on the ATP-induced peak increase in $[Ca^{2+}]_M$ in wild-type primary MEFs. (**D**) Dose-dependent decrease of the ATP-evoked peak $[Ca^{2+}]_M$ value in Rhod-2-loaded cells. Number of experiments performed is indicated on the columns. (**E**) Effect of increasing Rhod-2 concentrations (0, 10 and 30 µM) on cytosolic Ca^{2+} signaling in wild-type primary MEFs (see supplementary material Table S2). (**F**) Cytosolic Ca^{2+} measurements in PINK1 wild-type and PINK1-KO MEFs expressing mtLUC in the presence of 100 µM D-luciferin. 5 minutes after onset of D-luciferin perfusion, cytosolic Ca^{2+} responses were induced through addition of 1 mM ATP. Significantly increased basal cytosolic Ca^{2+} levels and a slower $[Ca^{2+}]_C$ removal were observed in PINK1-KO MEFs compared with control cells (see supplementary material Table S2). *P<0.05 vs control group.

KD and PINK1-KO cells cannot be explained by a reduced increase in overall $[Ca^{2+}]_C$. After reaching a peak value, $[Ca^{2+}]_C$ levels gradually declined again to pre-stimulatory levels. The rate of $[Ca^{2+}]_C$ decline was unaltered in PINK1-KD and PINK1-KO MEFs (Fig. 5A and supplementary material Table S2). This result was somewhat unexpected because of the marked reduction in the agonist-induced $[ATP]_M$ peak that we observed (see Fig. 4). To resolve this apparent discrepancy, we artificially lowered the $[Ca^{2+}]_M$ peak, to establish a dose-response relationship between $[Ca^{2+}]_M$ and the kinetics of cytosolic Ca^{2+} removal. Therefore, cells were stimulated in the presence of increasing concentrations of Rhod-2 because this cation has been demonstrated to decrease the amplitude of agonist-induced increase in $[Ca^{2+}]_M$ and as a consequence to reduce the mitochondrial ATP synthesis and cytosolic Ca^{2+} removal rate (Visch et al., 2006).

After pretreatment of control cells with increasing concentrations of Rhod-2, $[Ca^{2+}]_M$ and $[Ca^{2+}]_C$ were monitored in ATP-stimulated MEFs. Rhod-2 dose-dependently lowered the agonist-induced $[Ca^{2+}]_M$ peak in control MEFs (Fig. 5C,D). At 10 µM, the effect of Rhod-2 (~20% decrease) was comparable to results obtained with silencing of *Pink1* (compare with Fig. 3A to F). Similarly to depletion of PINK1, this concentration of Rhod-2 did not alter resting $[Ca^{2+}]_C$, the agonist-induced $[Ca^{2+}]_C$ peak or the rate of cytosolic Ca^{2+} removal (Fig. 5E and supplementary material Table S2). At 30 µM, however, Rhod-2 increased the resting $[Ca^{2+}]_C$, decreased the agonist-induced peak $[Ca^{2+}]_M$ by 80% and decreased the rate of cytosolic Ca^{2+} removal compared with control cells (Fig. 5C–E and supplementary material Table S2). Similar effects of Rhod-2 were obtained in N2a cells (supplementary material Table S3).

Next, because the reduction in the agonist-induced $[ATP]_M$ peak became apparent in stimulated cells in the presence of D-luciferin (see Fig. 4), we reasoned that similar conditions might be required to unmask potential problems with cytosolic Ca^{2+} handling. To test this possibility, we measured the rate of $[Ca^{2+}]_C$ decline in MEFs expressing mtLUC following stimulation in the presence of 100 µM D-luciferin to increase ATP consumption. Because the excitation spectra of Fura-2 and luciferin partially overlap, MEFs were loaded with the cytosolic Ca^{2+} indicator Fluo-4. Five minutes after onset of luciferin perfusion, $[Ca^{2+}]_C$ levels in resting PINK1-KO MEFs were significantly increased compared with the level in control cells, suggesting a decreased rate of cytosolic Ca^{2+} removal. When these MEFs were subsequently challenged with ATP, a similar peak $[Ca^{2+}]_C$ increase was observed in control and PINK1 KO MEFs which indicates that the size of the ER Ca^{2+} store is not altered after incubation for 5 minutes in the presence of D-luciferin. Mono-exponential fitting of the subsequent decrease of the Fluo-4 signal showed a significantly reduced rate of cytosolic Ca^{2+} removal in PINK1-KO MEFs, shown by an increased $t_{1/2}$ value in PINK1-KO MEFs (Fig. 5F and supplementary material Table S2).

We conclude that the decrease in mitochondrial ATP synthesis in PINK1-deficient cells is insufficient to alter cytosolic ATP-dependent processes such as Ca^{2+} extrusion after agonist stimulation. However, under conditions of increased ATP demand, PINK1-deficient cells are unable to produce sufficient amounts of ATP as reflected by decreased $[ATP]_M$ and decreased rates of cytosolic Ca^{2+} removal at rest and after stimulation.

Mitochondrial ATP levels are reduced in the brain of PINK1-deficient mice

Because mitochondrial ATP synthesis is severely impaired in PINK1-KO MEFs, we next asked whether this also holds true for the brains of these mice. We have previously shown that LVs encoding firefly luciferase enable long-term quantitative imaging of reporter gene expression in mouse brain using bioluminescence imaging (BLI) (Deroose et al., 2006). Because luciferase can only generate photons via oxidation of its substrate D-luciferin in the presence of ATP, we used the BLI signal as read-out to noninvasively monitor the mitochondrial ATP levels in the brain of living mice. Therefore, we injected LVs encoding mtLUC in the striatum of both *Pink1*$^{+/+}$ and *Pink1*$^{-/-}$ mice. Mice were monitored by BLI at 2, 4 and 6 weeks after injection. Images of all time points demonstrated a stable BLI signal originating from the striatum of both groups, but the bioluminescence signal was significantly lower (about 35%) in *Pink1*$^{-/-}$ mice (Fig. 6). In

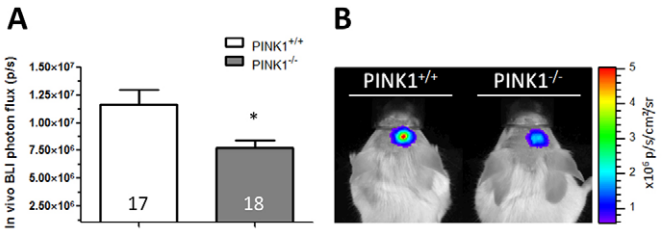

Fig. 6. Non-invasive bioluminescence imaging shows reduced mitochondrial ATP levels in the striatum of PINK1-KO mice. (**A**) In vivo BLI 4 weeks after stereotactic injection of 4 µl LV encoding mtLUC showed around 35% reduction of the BLI signal in PINK1-KO mice (n=18) compared with control mice (n=17). *P<0.05 vs control group. (**B**) A representative image of luciferase activity of one animal per group demonstrates the reduced BLI signal in PINK1-KO mice.

conclusion, the reduced ATP levels in vivo are compatible with the mitochondrial ATP synthesis deficit observed in primary PINK1-KO MEFs.

Discussion

Mitochondria are essential for cell survival because they are involved in energy metabolism, cell signaling and regulation of intracellular Ca^{2+} homeostasis. Several lines of evidence suggest a pivotal role of mitochondrial dysfunction in the pathogenesis of different human diseases, including Parkinson's disease (Abou-Sleiman et al., 2006). In this study, we investigated the physiological role of PINK1 in the function and structural integrity of mitochondria via specific depletion of PINK1 in cell culture and in the brain of mice. Both RNAi-mediated knockdown and genetic knockout of PINK1 induced a very similar mitochondrial phenotype, suggesting that, at least for the aspects of mitochondrial function we studied, no (additional) compensatory mechanisms occur in the primary PINK1-KO MEFs compared with PINK1-KD cells. Our findings support the conclusion that PINK1 has a key role in the regulation of mitochondrial function under basal and stimulated conditions.

Mitochondria are dynamic organelles whose morphology changes according to the energy requirements and health of the cell (Wasilewski and Scorrano, 2009). For this reason, a proper balance between mitochondrial fission and fusion is crucial to maintain normal mitochondrial function and thus cell homeostasis. Here, we demonstrate that depletion of PINK1 is paralleled with moderate mitochondrial fission and fragmentation, in agreement with other studies in PINK1-KD mammalian cells and in primary fibroblasts from patients with PD (Exner et al., 2007; Lutz et al., 2009; Sandebring et al., 2009; Weihofen et al., 2009; Wood-Kaczmar et al., 2008). This contrasts with findings in *Drosophila* where PINK1 promotes mitochondrial fission (Deng et al., 2008; Yang et al., 2008) and to a recent study in immortalized PINK1-KO MEFs, in which no changes in mitochondrial morphology were observed (Morais et al., 2009). These differences might reflect cell type-dependent metabolic differences between insect, primary and immortalized cells, which are known to affect mitochondrial morphology (Rossignol et al., 2004). Our study revealed that depletion of PINK1 not only induces mitochondrial fragmentation, but is also associated with a depolarized $\Delta\psi$. These data are compatible with the recently proposed model that mitochondrial fission segregates damaged mitochondria, which decreases their mitochondrial membrane potential, followed by selective targeting of these depolarized mitochondria by autophagy (Twig et al., 2008). However, because mitophagy is compromised in PINK1-deficient cells, these damaged mitochondria are cleared less efficiently, which was reflected by a slightly increased mitochondrial mass after silencing of *Pink1*. This also implies that mitochondrial fragmentation is rather secondary to the primary defect in mitophagic turnover.

$\Delta\psi$ is a key regulator of mitochondrial health and reflects the efficiency of proton extrusions across the inner mitochondrial membrane through the action of the OXPHOS complexes. In agreement with other studies (Gandhi et al., 2009; Piccoli et al., 2008; Wood-Kaczmar et al., 2008), we did not observe differences in maximal activity for the OXPHOS complexes in PINK1-KD or PINK1-KO cells. However, we cannot exclude the possibility that the OXPHOS system might operate less efficiently in resting PINK1-deficient cells, thus explaining the depolarized $\Delta\psi$. Although NAD(P)H levels were not significantly altered in these cells, a possible explanation could be a reduced supply of NADH by the TCA cycle. This suggests that the depolarized $\Delta\psi$ might be due to a reduced substrate delivery, as recently observed in PINK1-KD and PINK1-KO neurons (Gandhi et al., 2009). Other studies have reported that depletion of PINK1 reduces the activity of different OXPHOS complexes (Gautier et al., 2008; Gegg et al., 2009; Grunewald et al., 2009; Morais et al., 2009). However, the lack of selectivity for one of the complexes suggests that the reduced activity of the complexes might rather be an epiphenomenon of PINK1 silencing, possibly caused by mutations in the mitochondrial DNA as a result of sustained oxidative stress.

At the functional level, our study demonstrates that depletion of PINK1 significantly reduces agonist-stimulated Ca^{2+} entry into the mitochondrial matrix. To the best of our knowledge, this is the first report on direct $[Ca^{2+}]_M$ measurements in PINK1-KD or PINK1-KO cells. Mitochondrial Ca^{2+} dynamics is guided by the balance between Ca^{2+} influx through the highly selective Ca^{2+} uniporter (Kirichok et al., 2004) and Ca^{2+} extrusion through the Na^+- and H^+-dependent Ca^{2+} exchanger. Because the decay rate of Rhod-2 fluorescence to pre-stimulatory levels was similar in PINK1-KD, PINK1-KO and control cells, our findings suggest that silencing of PINK1 does not influence mitochondrial Ca^{2+} efflux, thereby indicating a normal functioning of this Ca^{2+} extrusion pathway. However, Ca^{2+} uptake in the mitochondrial matrix depends on the electrical driving force that is established by $\Delta\psi$ (Rutter and Rizzuto, 2000). Therefore, the lower agonist-induced mitochondrial Ca^{2+} peak level in the PINK1-deficient MEFs probably reflects the partial loss of $\Delta\psi$.

Live bioluminescence imaging of $[ATP]_M$ in unstimulated PINK1-depleted MEFs demonstrated a decreased ATP synthesis capacity under conditions of prolonged and/or increased ATP demand. This reduced ability to maintain basal $[ATP]_M$ levels in the presence of luciferase might be a consequence of increased ATP hydrolysis by complex V in the PINK1-KD or PINK1-KO conditions in an attempt to maintain the mitochondrial membrane potential (Gandhi et al., 2009; Morais et al., 2009).

It is well known that $[Ca^{2+}]_M$ allosterically triggers the enzymatic activity of the TCA cycle and complex V, resulting in increased NADH and $FADH_2$ levels, and subsequently, in an augmentation of the mitochondrial oxidative metabolism (Rutter and Rizzuto, 2000; Valsecchi et al., 2009). Because depletion of PINK1 induced a $\Delta\psi$ depolarization with a concomitant reduction of the agonist-stimulated increase in $[Ca^{2+}]_M$, we further demonstrated that silencing of *Pink1* also seriously decreased agonist-induced ATP

production. These data are in agreement with previous studies, showing that the agonist-induced peak increase in $[ATP]_M$ was reduced to half when the agonist-induced peak increase in $[Ca^{2+}]_M$ was reduced by no more than 30% (Jouaville et al., 1999). The observed deficit in ATP synthesis could be rescued by reintroduction of human WT PINK1, but not the PINK1 mutants (3xKD and W437X) in the PINK1-deficient cells. These data are in agreement with a recent study where PINK1 kinase activity (which is reduced or absent in the tested PINK1 mutants) proved essential for parkin binding and subsequent mitophagic clearance of damaged mitochondria (Geisler et al., 2010b). In addition, the reduced binding to the pro-apoptotic protein Beclin-1 reported for the W437X mutant might also interfere with proper activation of mitophagy (Michiorri et al., 2010).

Owing to the aberrations in ATP homeostasis, the fuelling of many ATP-requiring processes such as vesicle and organelle transport (Rintoul et al., 2006), macromolecule synthesis and degradation (Rabl et al., 2008) and maintenance of ATPase-mediated ion gradients (Pizzo and Pozzan, 2007) might become compromised. Somewhat surprisingly, the depletion of $[ATP]_M$ observed in the PINK1-deficient cells was insufficient to induce a reduction in cytosolic Ca^{2+} extrusion by SERCA and/or PMCA pumps, because the rate of cytosolic Ca^{2+} removal in stimulated cells was similar to that in control cells. However, when ATP consumption was stimulated by D-luciferin, $[Ca^{2+}]_C$ extrusion was slower in stimulated mtLUC-expressing PINK1-KO MEFs. This suggests that, under conditions of increased ATP demand, PINK1-KD and PINK1-KO MEFs cannot generate sufficient ATP for proper fuelling of ATP-demanding processes such as $[Ca^{2+}]_C$ extrusion. In dopaminergic neurons, reduced availability of ATP might lead even faster to a sustained increase in $[Ca^{2+}]_C$ levels, because these cells display autonomous pacemaking activity, resulting in a high ATP demand (Chan et al., 2010).

To corroborate the physiological relevance of our cell culture data, we performed in vivo bioluminescence imaging in the brain of adult *Pink1*$^{-/-}$ mice, which revealed a similar reduction in basal $[ATP]_M$ levels compared with that in age-matched *Pink1*$^{+/+}$ mice.

PINK1 and parkin act in a common pathway, with parkin being downstream of PINK1 (Clark et al., 2006; Park et al., 2006). These proteins appear to have an important role in mitochondrial quality control and specific disposal of damaged mitochondria via mitophagic clearance. During mitophagy, PINK1 selectively accumulates on depolarized mitochondria and thereby acts as a scaffold for the recruitment of parkin, leading to specific turnover of the dysfunctional mitochondria (Geisler et al., 2010a; Matsuda et al., 2010; Michiorri et al., 2010; Narendra et al., 2010; Vives-Bauza et al., 2010). Given the fact that depletion of PINK1 adversely affects this pathway, it is likely that defective mitochondria will accumulate inside PINK1-KD and PINK1-KO cells. Indeed, our data demonstrate that silencing of *Pink1* results in an increased number of fragmented and depolarized mitochondria. In addition, oxidative stress (ROS) is increased, which will further extend mitochondrial damage. As a consequence, mitochondrial Ca^{2+} influx becomes impaired, leading to reduced $[ATP]_M$ production and aberrant cytosolic Ca^{2+} signals. Of note, most of the data presented in this study were obtained in neuronal cell lines (N2A) and in primary fibroblasts, which showed very similar phenotypes. In the future, it will be interesting to explore different aspects of our findings in mouse brain or in primary neuronal cultures, but these measurements are technically challenging and will require further optimization.

In summary, our study provides evidence that PINK1 has an important role in maintenance of mitochondrial homeostasis in cells under physiological conditions. These data provide a better insight as to how loss of PINK1 function might lead to neurodegeneration in PD.

Materials and Methods

Generation of PINK1-knockout mice

The *Pink1* locus was targeted by homologous recombination in mouse E14.1 embryonic stem (ES) cells derived from 129/Ola mice. The targeting vector containing a 5′ homologous arm consisting of a 6.0 kb upstream genomic region of exon1 followed by the neomycin resistance gene, and a 2.2 kb 3′ homologous arm consisting of a part of intron1 at the 3′end was electroporated into ES cells. Neomycin-positive clones were selected and genotypically analyzed with the following primers: 5′-TCACACATCCAACCACGTTC-3′ (P1), 5′-CAGCGCATCGCCTTCTATC-3′ (P2), 5′-GTTCCATTGGCAACACCAC-3′ (P3) and 5′-TGCAATCCATCTTGTTCAA-TGG-3′ (P4). Microinjection of positive ES cells into the blastocysts of C57Bl/6J mice resulted in chimeric offspring. Mice containing the wild-type (*Pink1*$^{+/+}$) or the mutant (*Pink1*$^{+/-}$) *Pink1* allele were further bred to a C57Bl/6Jtyr^{c-2J} genetic background for at least four generations and finally intercrossed to obtain homozygous mutant mice (*Pink1*$^{-/-}$) with a homogenous background. All animal experiments were approved by the bioethics committee of K.U.Leuven.

Fibroblast cell culture

Pink1$^{+/+}$ and *Pink1*$^{-/-}$ mice were interbred. E13.5 embryos were dissected and heads and red organs were removed. The embryo bodies were repeatedly pushed through an 18 G needle in the presence of trypsin (Sigma). After incubation (5 minutes at 37°C), further disaggregation was performed using a 24 G needle. The single-cell suspension was seeded in Dulbecco's modified Eagle's medium (DMEM) with Glutamax (GIBCO BRL, Invitrogen), supplemented with 10% heat-inactivated fetal calf serum (FCS; Sigma), gentamicin (50 μg/ml; GIBCO BRL, Invitrogen) and 1% nonessential amino acids (GIBCO) and cultured at 37°C in a humidified atmosphere containing 5% CO_2. The primary MEFs could be cultured up to eight passages. In some experiments, MEFs were cultured in galactose-containing medium (DMEM deprived of glucose) supplemented with 10 mM galactose, 4 mM glutamine, 1 mM sodium pyruvate, 10% dialyzed FCS and gentamycin) for six consecutive days. Mouse N2a cells were cultured in similar conditions to MEFs, but without addition of nonessential amino acids to the medium. These N2a cells were not differentiated before experiments were performed.

Cloning of transfer plasmids

PINK1 knockdown was achieved with lentiviral vector (LV)-based vectors encoding modified miRNA30-based short-hairpin (sh) sequences against two different regions in mouse PINK1 (supplementary material Table S1) and a blasticidin-resistance cassette (Sun et al., 2006). Functionality of the sh2PINK1 sequence has been previously validated (Zhou et al., 2007). As a negative control, a four nucleotide mismatch (MM) miRNA30-based short-hairpin sequence was designed. Mitochondrial targeted aequorin (mtAEQ), luciferase (mtLUC) (provided by Rosario Rizzuto, University of Ferrara, Italy) and eGFP (mtGFP) were PCR amplified and cloned in a LV transfer plasmid upstream of an IRES-hygromycin B resistance gene. cDNA of human WT *PINK1* and two recessive mutants (W437X and triple kinase-dead, 3xKD) (gift from Philipp J. Kahle, University of Tübingen, Germany) was cloned in a LV transfer plasmid upstream of an IRES-puromycin cassette.

LV production and transduction

LV production was performed as described previously (Ibrahimi et al., 2009). Cells were transduced with LV diluted in the cell culture medium. After 72 hours, vector-containing medium was replaced by medium with blasticidin (12 μg/ml, Invitrogen), hygromycin B (200 μg/ml, Invitrogen) or puromycin (3 μg/ml, Invitrogen) to select for transduced cells.

Quantitative PCR

To determine *Pink1* mRNA levels in transduced cells, 5 μg total RNA was reverse-transcribed using the High Capacity cDNA Archive Kit (Applied Biosystems) and cDNA was used in quadruplicate as template for quantitative PCR (Q-PCR) amplification with Taqman® probe based detection, as described previously (Taymans et al., 2006). The *Pink1* mRNA levels were normalized to levels of *Gapdh* mRNA.

Luminescence monitoring of mitochondrial Ca^{2+} and mitochondrial ATP

Changes in the free mitochondrial $[Ca^{2+}]$ ($[Ca^{2+}]_M$) and [ATP] ($[ATP]_M$) in N2a and MEF cells were determined by luminometry (Visch et al., 2006). Briefly, to monitor luminescence of mtLUC, coverslips were placed in the 37°C thermostated luminometer and perfused (3 ml/minute) with HEPES–Tris (HT) buffer containing 100 μM D-luciferin (Xenogen). At the end of each experiment, cells were lysed with 100 μM digitonin in the presence of 10 mM Mg-ATP to determine the maximal mtLUC signal which was set at 100% (Valsecchi et al., 2009). Light output was integrated during 1 second and recorded at intervals of 2 seconds. The same custom-

built set-up was used to monitor mtAEQ photon emission. Before $[Ca^{2+}]_M$ measurements, mtAEQ was reconstituted with 5 μM native coelenterazine (Invitrogen) in DMEM medium for 1 hour at 37°C. Cells were perfused with KREBS medium, followed by lysis in Ca^{2+}-rich medium (100 μM digitonin and 10 mM $CaCl_2$ in H_2O) to calibrate the luminescence data. mtAEQ photon emission was converted off-line into $[Ca^{2+}]_M$ values, using a computer algorithm (Brini et al., 1995).

Fluorescence imaging of the cytosolic free-Ca^{2+} levels

Cells were loaded with 3 μM Fura-2 (Invitrogen) (25 minutes, 37°C) to quantify changes in free cytosolic $[Ca^{2+}]$ ($[Ca^{2+}]_C$) (Visch et al., 2006). After thorough washing with HT buffer, coverslips were mounted in a temperature-controlled (37°C) superfusion chamber attached to the stage of an inverted microscope (Axiovert 200 M; Zeiss) equipped with a 40× NA1.25 Plan NeoFluar objective. Fura-2 was excited at 340 and 380 nm alternately using a monochromator (Polychrome IV; TILL Photonics). Fluorescence emission light was directed by a 415DCLP dichroic mirror (Omega Optical) through a 510WB40 emission filter on a CoolSNAP HQ monochrome CCD camera (Roper Scientific). A camera exposure time of 200 mseconds and interframe interval of 1 second were used. To quantify $[Ca^{2+}]_C$ signals in the presence of D-luciferin, cells were loaded with 2.5 μM Fluo-4 and imaged using a 505DRLPXR dichroic mirror and a 515ALP emission filter (camera exposure time: 200 mseconds; interframe interval: 1 second). At the end of each measurement, cells were scraped off the coverslip to allow correction for background fluorescence. Changes in $[Ca^{2+}]_C$ were evoked in N2a cells and MEFs by superfusion with bradykinin (BK; 1 μM) or ATP (1 mM), respectively. The kinetics of Ca^{2+} removal after cell stimulation were fitted to a mono-exponential equation: $y(t)=y_0+y_{max}\cdot e^{-\lambda t}$, where λ is the decay time constant, y_{max} represents the maximal Fura-2 ratio signal after stimulation and y_0 is the basal ratio to which $y(t)$ declines. The halftime ($t_{1/2}$) was given by: $t_{1/2}\,(s)=-\ln(0.5)\cdot\lambda$.

Fluorescence imaging of the mitochondrial free-Ca^{2+} levels

To measure $[Ca^{2+}]_M$, MEFs were incubated with the mitochondria-specific Ca^{2+}-sensitive cation Rhod-2 (3 μM, 25 minutes, 37°C, Invitrogen) and visualized using the same microscopy system as used for Fura-2. Before Rhod-2 loading, cells were transduced with LV encoding mtGFP allowing automated quantitative assessment of mitochondria-specific Rhod-2 emission intensity (Koopman et al., 2008). For fluorescence imaging, a 63× NA 1.25 Plan NeoFluar objective was used. Rhod-2 and mtGFP were alternately excited at 540 and 470 nm. Emission light was directed by 560DRLP (Rhod-2) or 510WB40 (mtGFP) dichroic mirrors and 565ALP (Rhod-2) or 515ALP (mtGFP) emission filters to the CCD camera. At the end of each measurement, cells were scraped off the coverslip to allow correction for background fluorescence.

Real-time imaging of intracellular NAD(P)H fluorescence

Intracellular NAD(P)H autofluorescence was determined as described previously (Visch et al., 2006). NAD(P)H was excited at 360 nm and fluorescence emission was directed by a 415DCLP dichroic mirror through a 510WB40 emission filter onto the CCD camera (routinely, ten fields of cells were imaged per coverslip). Subsequently, the same cells were treated with the complex I inhibitor rotenone (100 nM, 5 minutes) and again 10 fields of cells were imaged. The mean NAD(P)H autofluorescence intensity was quantified in an intracellular, mitochondria-dense, region of interest and in an extracellular region of the same size to correct for background signals.

Live cell imaging of mitochondrial membrane potential and morphology

To assess mitochondrial membrane potential and morphology, cells were incubated with the mitochondria-specific cation tetramethyl Rhodamine methyl ester (TMRM, 100 nM, 25 minutes, 37°C, Invitrogen). TMRM loading was carried out in the presence of 1 μM cyclosporin H to exhibit dye extrusion by P-glycoprotein. Fluorescence imaging was performed with the microscopy system using the settings described for Rhod-2. Routinely, ten fields of cells were analyzed per coverslip. Mitochondrial membrane potential ($\Delta\psi$) and morphology were assessed using an established unbiased quantification approach (Koopman et al., 2008). This approach allowed calculation of the mean TMRM fluorescence intensity for each mitochondrial object, the number of mitochondria per cell (N_c), mitochondrial area (A_M), mitochondrial mass (M_M, given by the product of N_C and A_M) and mitochondrial form factor (F). Mitochondrial mass was also determined in fixed MEFs. After immunocytochemistry, total fluorescent TOM-20 signal per cell was automatically quantified with the IN cell analyzer 1000 (GE healthcare), as recently described (Gerard et al., 2010).

Live cell quantification of ROS-induced hydroethidine oxidation

To assess the rate of reactive oxygen species (ROS)-induced hydroethidine (HEt) oxidation, cells were incubated with HT medium containing HEt (10 μM, 10 minutes, 37°C; Invitrogen). Fluorescence imaging was carried out with the microscopy system described above using 490 nm excitation light, a 40× NA1.25 Plan NeoFluar objective, a 525DRLP dichroic mirror and a 565ALP emission filter. Routinely, ten fields of cells were analyzed on each coverslip by quantifying the background-corrected mean fluorescence intensity in a cytosolic and mitochondria-rich region.

Biochemical analysis of oxidative phosphorylation complex activity

Measurement of the activities of the mitochondrial respiratory chain enzymes (Complex I to Complex V) and citrate synthase (CS) was determined in mitochondria-enriched fractions of MEFs and N2a cells, as described previously (Rodenburg, 2010). The specific activity of each enzyme was normalized to protein concentration and expressed as a percentage of the control.

Blue native PAGE, western blot analysis and in-gel activity measurement

Mitochondrial-enriched protein fractions were isolated from ~3×10^6 cultured cells (Calvaruso et al., 2008) and loaded on Bis-Tris gels for blue native PAGE and western blotting. Immunoblots were incubated with the following primary antibodies (1 μg/ml): anti-complex-I subunit NDUFA9, anti-complex-II subunit 70 kDa Fp (Invitrogen), anti-complex-III core2, anti-complex-IV subunit I, anti-ATP-synthase subunit alpha (Mitosciences) (Nijtmans et al., 2002). Detection of PINK1 was performed with a specific antibody against PINK1 (Novus Biologicals, BC-494, 1:2000 dilution), including a VDAC1 antibody (Calbiochem, 1:10000 dilution) to control for equal loading. In-gel activity of complex I was determined after overnight incubation at room temperature in 2 mM Tris-HCl pH 7.4, 0.1 mg/ml NADH, and 2.5 mg/ml Nitrotetrazolium Blue (Sigma). Gels were washed in distilled water and scanned immediately with the Odyssey Imaging system (Li-Cor).

Immunocytochemistry

Cells were grown on 12-mm-diameter coverslips and fixed with 4% formaldehyde. After blocking with 10% goat serum in PBS, cells were incubated for 2 hours with primary antibody [1:100 anti-PINK1 (Novus biologicals) and 1:300 anti-TOM-20 (Santa Cruz Biotechnology, FL-145)] in PBS plus 10% goat serum. After washing with PBS, the cells were incubated for 1 hour with secondary antibody (1:500 Alexa-Fluor-488-conjugated antibodies; Invitrogen). Thereafter, the coverslips were mounted on a microscope slide with Mowiol solution (Sigma). Fluorescence was detected with the 488 argon-ion laser with a laser scanning microscopy unit (LSM 510; Carl Zeiss).

Stereotactic surgery

Stereotactic injection of LV was performed in the striatum of adult C57Bl/6Jtyr^{c-2J} female *Pink1*$^{+/+}$ and *Pink1*$^{-/-}$ mice (Deroose et al., 2006). The following coordinates were used: anteroposterior, 0.5 mm; lateral, 2.0 mm; dorsoventral, 3.0–2.0 mm. 4 μl of highly concentrated vector (7×10^7 pg p24/ml) was injected at a rate of 0.25 μl/minute.

In vivo bioluminescence imaging

The mice were imaged in an IVIS 100 system (Xenogen, Alameda, CA) as described previously (Deroose et al., 2006). The animals were injected intravenously with D-luciferin (126 mg/kg; Xenogen) dissolved in PBS (15 mg/ml). Subsequently, 1 minute frames were acquired until the maximal signal was reached. The data are reported as the photon flux (photons/second) from a 1.6 cm^2 circular region of interest.

Image analysis and statistics

Images were processed and analyzed using Image Pro Plus 6.3 software (Media Cybernetics). Statistical analysis and curve fitting were performed using Origin Pro 7.5 (Originlabs). Results from multiple experiments are expressed as mean ± s.e.m. and statistical significance was assessed using the Student's *t*-test (Bonferroni corrected) or ANOVA with post-hoc Dunn's test for intergroup comparisons. Statistical significance level was set as follows: *P<0.05, **P<0.01, ***P<0.001.

The authors thank Marly Balcer and Frea Coun for excellent technical assistance with the lentiviral vector production and Sjenet E. Van Emst–de Vries for excellent help with blue native PAGE, western blot analysis and in-gel activity measurements. Research was funded by the Michael J. Fox Foundation (Fast Track grant), the European FP6 NoE DiMI LSHB-CT-2005-512146, the FWO Vlaanderen (project G.0406.06, doctoral fellowship to B.H., postdoctoral fellowship to C.V.dH.), the IWT-Vlaanderen (IWT/SBO 80020, doctoral fellowship to S.-A.A.), the Queen Elisabeth Medical Foundation, the K. U. Leuven OT/08/052A, IOF-KP/07/001, Center of Excellence 'MoSAIC' (EF/05/08) and an equipment grant from NWO (No: 911-02-008).

Supplementary material available online at
http://jcs.biologists.org/cgi/content/full/124/7/1115/DC1

References

Abou-Sleiman, P. M., Muqit, M. M. and Wood, N. W. (2006). Expanding insights of mitochondrial dysfunction in Parkinson's disease. *Nat. Rev. Neurosci.* **7**, 207-219.

Bender, A., Krishnan, K. J., Morris, C. M., Taylor, G. A., Reeve, A. K., Perry, R. H., Jaros, E., Hersheson, J. S., Betts, J., Klopstock, T. et al. (2006). High levels of mitochondrial DNA deletions in substantia nigra neurons in aging and Parkinson disease. *Nat. Genet.* **38**, 515-517.

Brini, M., Marsault, R., Bastianutto, C., Alvarez, J., Pozzan, T. and Rizzuto, R. (1995). Transfected aequorin in the measurement of cytosolic Ca2+ concentration ([Ca2+]c). A critical evaluation. *J. Biol. Chem.* **270**, 9896-9903.

Calvaruso, M. A., Smeitink, J. and Nijtmans, L. (2008). Electrophoresis techniques to investigate defects in oxidative phosphorylation. *Methods* **46**, 281-287.
Chan, C. S., Gertler, T. S. and Surmeier, D. J. (2010). A molecular basis for the increased vulnerability of substantia nigra dopamine neurons in aging and Parkinson's disease. *Mov. Disord.* **25 Suppl. 1**, S63-S70.
Clark, I. E., Dodson, M. W., Jiang, C., Cao, J. H., Huh, J. R., Seol, J. H., Yoo, S. J., Hay, B. A. and Guo, M. (2006). Drosophila pink1 is required for mitochondrial function and interacts genetically with parkin. *Nature* **441**, 1162-1166.
Dagda, R. K., Cherra, S. J., 3rd, Kulich, S. M., Tandon, A., Park, D. and Chu, C. T. (2009). Loss of PINK1 function promotes mitophagy through effects on oxidative stress and mitochondrial fission. *J. Biol. Chem.* **284**, 13843-13855.
Deng, H., Jankovic, J., Guo, Y., Xie, W. and Le, W. (2005). Small interfering RNA targeting the PINK1 induces apoptosis in dopaminergic cells SH-SY5Y. *Biochem. Biophys. Res. Commun.* **337**, 1133-1138.
Deng, H., Dodson, M. W., Huang, H. and Guo, M. (2008). The Parkinson's disease genes pink1 and parkin promote mitochondrial fission and/or inhibit fusion in Drosophila. *Proc. Natl. Acad. Sci. USA* **105**, 14503-14508.
Deroose, C. M., Reumers, V., Gijsbers, R., Bormans, G., Debyser, Z., Mortelmans, L. and Baekelandt, V. (2006). Noninvasive monitoring of long-term lentiviral vector-mediated gene expression in rodent brain with bioluminescence imaging. *Mol. Ther.* **14**, 423-431.
Exner, N., Treske, B., Paquet, D., Holmstrom, K., Schiesling, C., Gispert, S., Carballo-Carbajal, I., Berg, D., Hoepken, H. H., Gasser, T. et al. (2007). Loss-of-function of human PINK1 results in mitochondrial pathology and can be rescued by parkin. *J. Neurosci.* **27**, 12413-12418.
Forkink, M., Smeitink, J. A., Brock, R., Willems, P. H. and Koopman, W. J. (2010). Detection and manipulation of mitochondrial reactive oxygen species in mammalian cells. *Biochim. Biophys. Acta* **1797**, 1034-1044.
Gandhi, S., Wood-Kaczmar, A., Yao, Z., Plun-Favreau, H., Deas, E., Klupsch, K., Downward, J., Latchman, D. S., Tabrizi, S. J., Wood, N. W. et al. (2009). PINK1-associated Parkinson's disease is caused by neuronal vulnerability to calcium-induced cell death. *Mol. Cell* **33**, 627-638.
Gasser, T. (2009). Molecular pathogenesis of Parkinson disease: insights from genetic studies. *Expert Rev. Mol. Med.* **11**, e22.
Gautier, C. A., Kitada, T. and Shen, J. (2008). Loss of PINK1 causes mitochondrial functional defects and increased sensitivity to oxidative stress. *Proc. Natl. Acad. Sci. USA* **105**, 11364-11369.
Gegg, M. E., Cooper, J. M., Schapira, A. H. and Taanman, J. W. (2009). Silencing of PINK1 expression affects mitochondrial DNA and oxidative phosphorylation in dopaminergic cells. *PLoS One* **4**, e4756.
Geisler, S., Holmstrom, K. M., Skujat, D., Fiesel, F. C., Rothfuss, O. C., Kahle, P. J. and Springer, W. (2010a). PINK1/Parkin-mediated mitophagy is dependent on VDAC1 and p62/SQSTM1. *Nat. Cell Biol.* **12**, 119-131.
Geisler, S., Holmstrom, K. M., Treis, A., Skujat, D., Weber, S. S., Fiesel, F. C., Kahle, P. J. and Springer, W. (2010b). The PINK1/Parkin-mediated mitophagy is compromised by PD-associated mutations. *Autophagy* **6**, 871-878.
Gerard, M., Deleersnijder, A., Daniels, V., Schreurs, S., Munck, S., Reumers, V., Pottel, H., Engelborghs, Y., Van den Haute, C., Taymans, J. M. et al. (2010). Inhibition of FK506 binding proteins reduces alpha-synuclein aggregation and Parkinson's disease-like pathology. *J. Neurosci.* **30**, 2454-2463.
Grunewald, A., Gegg, M. E., Taanman, J. W., King, R. H., Kock, N., Klein, C. and Schapira, A. H. (2009). Differential effects of PINK1 nonsense and missense mutations on mitochondrial function and morphology. *Exp. Neurol.* **219**, 266-273.
Ibrahimi, A., Vande Velde, G., Reumers, V., Toelen, J., Thiry, I., Vandeputte, C., Vets, S., Deroose, C., Bormans, G., Baekelandt, V. et al. (2009). Highly efficient multicistronic lentiviral vectors with peptide 2A sequences. *Hum. Gene Ther.* **20**, 845-860.
Jouaville, L. S., Pinton, P., Bastianutto, C., Rutter, G. A. and Rizzuto, R. (1999). Regulation of mitochondrial ATP synthesis by calcium: evidence for a long-term metabolic priming. *Proc. Natl. Acad. Sci. USA* **96**, 13807-13812.
Kirichok, Y., Krapivinsky, G. and Clapham, D. E. (2004). The mitochondrial calcium uniporter is a highly selective ion channel. *Nature* **427**, 360-364.
Koopman, W. J., Verkaart, S., Visch, H. J., van der Westhuizen, F. H., Murphy, M. P., van den Heuvel, L. W., Smeitink, J. A. and Willems, P. H. (2005). Inhibition of complex I of the electron transport chain causes O2-. -mediated mitochondrial outgrowth. *Am. J. Physiol. Cell Physiol.* **288**, C1440-C1450.
Koopman, W. J., Distelmaier, F., Esseling, J. J., Smeitink, J. A. and Willems, P. H. (2008). Computer-assisted live cell analysis of mitochondrial membrane potential, morphology and calcium handling. *Methods* **46**, 304-311.
Langston, J. W., Ballard, P., Tetrud, J. W. and Irwin, I. (1983). Chronic Parkinsonism in humans due to a product of meperidine-analog synthesis. *Science* **219**, 979-980.
Lutz, A. K., Exner, N., Fett, M. E., Schlehe, J. S., Kloos, K., Lammermann, K., Brunner, B., Kurz-Drexler, A., Vogel, F., Reichert, A. S. et al. (2009). Loss of parkin or PINK1 function increases Drp1-dependent mitochondrial fragmentation. *J. Biol. Chem.* **284**, 22938-22951.
Matsuda, N., Sato, S., Shiba, K., Okatsu, K., Saisho, K., Gautier, C. A., Sou, Y. S., Saiki, S., Kawajiri, S., Sato, F. et al. (2010). PINK1 stabilized by mitochondrial depolarization recruits Parkin to damaged mitochondria and activates latent Parkin for mitophagy. *J. Cell Biol.* **189**, 211-221.
Michiorri, S., Gelmetti, V., Giarda, E., Lombardi, F., Romano, F., Marongiu, R., Nerini-Molteni, S., Sale, P., Vago, R., Arena, G. et al. (2010). The Parkinson-associated protein PINK1 interacts with Beclin1 and promotes autophagy. *Cell Death Differ.* **17**, 962-974.
Morais, V. A., Verstreken, P., Roethig, A., Smet, J., Snellinx, A., Vanbrabant, M., Haddad, D., Frezza, C., Mandemakers, W., Vogt-Weisenhorn, D. et al. (2009). Parkinson's disease mutations in PINK1 result in decreased Complex I activity and deficient synaptic function. *EMBO Mol. Med.* **1**, 99-111.
Narendra, D. P., Jin, S. M., Tanaka, A., Suen, D. F., Gautier, C. A., Shen, J., Cookson, M. R. and Youle, R. J. (2010). PINK1 is selectively stabilized on impaired mitochondria to activate Parkin. *PLoS Biol.* **8**, e1000298.
Nicholls, D. G. and Ward, M. W. (2000). Mitochondrial membrane potential and neuronal glutamate excitotoxicity: mortality and millivolts. *Trends Neurosci.* **23**, 166-174.
Nijtmans, L. G., Henderson, N. S. and Holt, I. J. (2002). Blue Native electrophoresis to study mitochondrial and other protein complexes. *Methods* **26**, 327-334.
Park, J., Lee, S. B., Lee, S., Kim, Y., Song, S., Kim, S., Bae, E., Kim, J., Shong, M., Kim, J. M. et al. (2006). Mitochondrial dysfunction in Drosophila PINK1 mutants is complemented by parkin. *Nature* **441**, 1157-1161.
Piccoli, C., Sardanelli, A., Scrima, R., Ripoli, M., Quarato, G., D'Aprile, A., Bellomo, F., Scacco, S., De Michele, G., Filla, A. et al. (2008). Mitochondrial respiratory dysfunction in familiar parkinsonism associated with PINK1 mutation. *Neurochem. Res.* **33**, 2565-2574.
Pizzo, P. and Pozzan, T. (2007). Mitochondria-endoplasmic reticulum choreography: structure and signaling dynamics. *Trends Cell Biol.* **17**, 511-517.
Rabl, J., Smith, D. M., Yu, Y., Chang, S. C., Goldberg, A. L. and Cheng, Y. (2008). Mechanism of gate opening in the 20S proteasome by the proteasomal ATPases. *Mol. Cell* **30**, 360-368.
Rintoul, G. L., Bennett, V. J., Papaconstandinou, N. A. and Reynolds, I. J. (2006). Nitric oxide inhibits mitochondrial movement in forebrain neurons associated with disruption of mitochondrial membrane potential. *J. Neurochem.* **97**, 800-806.
Rizzuto, R., Simpson, A. W., Brini, M. and Pozzan, T. (1992). Rapid changes of mitochondrial Ca^{2+} revealed by specifically targeted recombinant aequorin. *Nature* **358**, 325-327.
Rodenburg, R. J. (2010). Biochemical diagnosis of mitochondrial disorders. *J. Inherit. Metab. Dis*. (Epub ahead of print).
Rossignol, R., Gilkerson, R., Aggeler, R., Yamagata, K., Remington, S. J. and Capaldi, R. A. (2004). Energy substrate modulates mitochondrial structure and oxidative capacity in cancer cells. *Cancer Res.* **64**, 985-993.
Rutter, G. A. and Rizzuto, R. (2000). Regulation of mitochondrial metabolism by ER Ca^{2+} release: an intimate connection. *Trends Biochem. Sci.* **25**, 215-221.
Sandebring, A., Thomas, K. J., Beilina, A., van der Brug, M., Cleland, M. M., Ahmad, R., Miller, D. W., Zambrano, I., Cowburn, R. F., Behbahani, H. et al. (2009). Mitochondrial alterations in PINK1 deficient cells are influenced by calcineurin-dependent dephosphorylation of dynamin-related protein 1. *PLoS One* **4**, e5701.
Schapira, A. H., Cooper, J. M., Dexter, D., Jenner, P., Clark, J. B. and Marsden, C. D. (1989). Mitochondrial complex I deficiency in Parkinson's disease. *Lancet* **1**, 1269.
Sun, D., Melegari, M., Sridhar, S., Rogler, C. E. and Zhu, L. (2006). Multi-miRNA hairpin method that improves gene knockdown efficiency and provides linked multi-gene knockdown. *Biotechniques* **41**, 59-63.
Taymans, J. M., Van den Haute, C. and Baekelandt, V. (2006). Distribution of PINK1 and LRRK2 in rat and mouse brain. *J. Neurochem.* **98**, 951-961.
Twig, G., Elorza, A., Molina, A. J., Mohamed, H., Wikstrom, J. D., Walzer, G., Stiles, L., Haigh, S. E., Katz, S., Las, G. et al. (2008). Fission and selective fusion govern mitochondrial segregation and elimination by autophagy. *EMBO J.* **27**, 433-446.
Valente, E. M., Abou-Sleiman, P. M., Caputo, V., Muqit, M. M., Harvey, K., Gispert, S., Ali, Z., Del Turco, D., Bentivoglio, A. R., Healy, D. G. et al. (2004). Hereditary early-onset Parkinson's disease caused by mutations in PINK1. *Science* **304**, 1158-1160.
Valsecchi, F., Esseling, J. J., Koopman, W. J. and Willems, P. H. (2009). Calcium and ATP handling in human NADH: ubiquinone oxidoreductase deficiency. *Biochim. Biophys. Acta* **1792**, 1130-1137.
Visch, H. J., Rutter, G. A., Koopman, W. J., Koenderink, J. B., Verkaart, S., de Groot, T., Varadi, A., Mitchell, K. J., van den Heuvel, L. P., Smeitink, J. A. et al. (2004). Inhibition of mitochondrial Na^{+}-Ca^{2+} exchange restores agonist-induced ATP production and Ca^{2+} handling in human complex I deficiency. *J. Biol. Chem.* **279**, 40328-40336.
Visch, H. J., Koopman, W. J., Zeegers, D., van Emst-de Vries, S. E., van Kuppeveld, F. J., van den Heuvel, L. W., Smeitink, J. A. and Willems, P. H. (2006). Ca^{2+}-mobilizing agonists increase mitochondrial ATP production to accelerate cytosolic Ca^{2+} removal: aberrations in human complex I deficiency. *Am. J. Physiol. Cell Physiol.* **291**, C308-C316.
Vives-Bauza, C., Zhou, C., Huang, Y., Cui, M., de Vries, R. L., Kim, J., May, J., Tocilescu, M. A., Liu, W., Ko, H. S. et al. (2010). PINK1-dependent recruitment of Parkin to mitochondria in mitophagy. *Proc. Natl. Acad. Sci. USA* **107**, 378-383.
Wasilewski, M. and Scorrano, L. (2009). The changing shape of mitochondrial apoptosis. *Trends Endocrinol. Metab.* **20**, 287-294.
Weihofen, A., Thomas, K. J., Ostaszewski, B. L., Cookson, M. R. and Selkoe, D. J. (2009). Pink1 forms a multiprotein complex with Miro and Milton, linking Pink1 function to mitochondrial trafficking. *Biochemistry* **48**, 2045-2052.
Wood-Kaczmar, A., Gandhi, S., Yao, Z., Abramov, A. Y., Miljan, E. A., Keen, G., Stanyer, L., Hargreaves, I., Klupsch, K., Deas, E. et al. (2008). PINK1 is necessary for long term survival and mitochondrial function in human dopaminergic neurons. *PLoS One* **3**, e2455.
Yang, Y., Ouyang, Y., Yang, L., Beal, M. F., McQuibban, A., Vogel, H. and Lu, B. (2008). Pink1 regulates mitochondrial dynamics through interaction with the fission/fusion machinery. *Proc. Natl. Acad. Sci. USA* **105**, 7070-7075.
Zhou, C., Huang, Y., Shao, Y., May, J., Prou, D., Perier, C., Dauer, W., Schon, E. A. and Przedborski, S. (2008). The kinase domain of mitochondrial PINK1 faces the cytoplasm. *Proc. Natl. Acad. Sci. USA* **105**, 12022-12027.
Zhou, H., Falkenburger, B. H., Schulz, J. B., Tieu, K., Xu, Z. and Xia, X. G. (2007). Silencing of the Pink1 gene expression by conditional RNAi does not induce dopaminergic neuron death in mice. *Int. J. Biol. Sci.* **3**, 242-250.

Journal of Cell Science

Table S1. Overview of the short-hairpin PINK1 sense strands

shRNA	shRNA targeting sequence on PINK1 mRNA
sh1PINK1	1548 – AGCCCTGAAGAATCTGAAATT - 1568
sh1PINK1MM	1548 – AGCCCTGAACTTACTGAAATT - 1568
sh2PINK1	757 – GGAGCAGTTACTTACAGAAGA - 777

RNAi-mediated knockdown of PINK1 was induced by two miRNA30-based short hairpin sequences directed against different regions of the mouse PINK1 mRNA. The shRNA targeting sequences on the PINK1 mRNA are shown, when the translation start-site is set at position 1. Due to complementation of the central 4 nucleotides of sh1PINK1, PINK1 mRNA was no longer recognized by the sense strand of the shPINK1MM.